JOURNAL OF Materials CHEMISTRY

Crystallization mechanism of Al-TS-1 synthesised from amorphous wetness-impregnated Al_2O_3–TiO_2–SiO_2 xerogels: role of aluminium species

Juan A. Melero,* Rafael van Grieken, David P. Serrano and Juan J. Espada

Department of Experimental Sciences and Engineering, School of Experimental Sciences and Technology, Rey Juan Carlos University, 28933 Mostoles, Madrid, Spain.
E-mail: j.melero@escet.urjc.es

Received 24th November 2000, Accepted 7th February 2001
First published as an Advance Article on the web 15th March 2001

The crystallization mechanism of Al-TS-1 zeolite has been investigated using amorphous wetness-impregnated Al_2O_3–TiO_2–SiO_2 xerogels as raw materials. Samples with different degrees of crystallinity have been prepared and characterised by means of conventional techniques. The catalytic activity of the Ti and Al centres along with the crystallization have been tested by oxyfunctionalization of n-hexane with H_2O_2 and alcohol etherification reactions, respectively. The crystallization mechanism involves a partial dissolution of the initial xerogel, which is more pronounced for Si and Ti species, whereas Al species remain in a high percentage within the solid. Simultaneously, the starting polymeric cogel is converted into a particulate amorphous material formed by a tight packing of primary units, which are aggregated leading to secondary particles that become independent of the cogel as they reach a critical size of 0.5 μm. During this aggregation process, the crystallization is governed by solid–solid transformations without any incorporation of species from the solution. The last crystallization stage is characterised by a slow incorporation of different species from the solution accompanied with an increase in the solid yield and a complete incorporation of Al species, which results in a densification of the secondary particles and their transformation into zeolite crystals. In addition, the environment of Ti and Al atoms is modified by the crystallization affecting significantly their catalytic activity. The aluminium content in the starting xerogel has an important influence on the crystallization process, with enhancement of the Ti and Si species dissolution as the Al content increases in the raw material. Moreover, a higher participation of the solution-mediated process in the global zeolite crystallization and a decrease of the Ti content in the final crystalline materials are evidenced with increasing Al content in the initial xerogel.

1 Introduction

Since the discovery of TS-1 as a suitable catalyst in selective oxidation reactions with hydrogen peroxide,[1–7] serious research efforts have been devoted to the incorporation of another ion along with Ti^{4+} into the zeolite framework to enlarge their catalytic applications. Coincorporation of Ti and trivalent elements such as Al^{3+}, Ga^{3+}, Fe^{3+} and B^{3+} in MFI and MEL structures has been reported.[8–13]

Most of the methods reported in the literature for Al-TS-1 preparation[8–10] are based on the hydrothermal crystallization of a hydrogel obtained from basic hydrolysis of the respective precursors with aqueous tetrapropylammonium hydroxide (TPAOH). In a series of papers,[12–14] we have described an alternative and simpler method to incorporate simultaneously Ti and Al into the MFI framework, based on previous works dealing with TS-1 synthesis by wetness impregnation of TiO_2–SiO_2 xerogels.[15–17] This improved method involves the hydrothermal crystallization of wetness-impregnated amorphous Al_2O_3–TiO_2–SiO_2 solids with TPAOH aqueous solutions under autogenous pressure at 170 °C. Additionally, the bifunctional properties of this material have been successfully applied for MTBE synthesis from isobutane and methanol through both oxidising and acid-catalysed steps on a single catalytic system.[18,19]

The conventional mechanism postulated for zeolite synthesis is viewed as a two step process: nucleation (formation of first crystalline entities) and crystal growth around these nuclei. However, in previous works dealing with the synthesis of TS-1 and TS-2 zeolites from amorphous wetness-impregnated TiO_2–SiO_2 xerogels,[20,21] we have found that the conventional mechanism is not valid and the crystallization proceeds mainly through solid–solid transformations. On the other hand, recent studies focused on the crystallization mechanism of Al-Ti-beta synthesised from amorphous xerogels wetness-impregnated with aqueous TEAOH solutions have shown that the crystallization is different from that observed for TS-1 and TS-2 zeolites.[22] The mechanism observed involves complete dissolution of the initial xerogel and the subsequent formation of an amorphous gel consisting of primary particles, which are packing in secondary pseudo-crystalline entities that finally yield Ti-beta crystals through a densification and zeolitization process. In this last stage the incorporation of soluble species is also detected. For this system, Al species play an essential role in the formation of the Ti-beta phase. Therefore, the objectives of this research were to investigate the mechanism prevailing in the crystallization of Al-TS-1 from amorphous wetness-impregnated Al_2O_3–TiO_2–SiO_2 xerogels when aqueous TPAOH solutions are used as templating agent, and to the determine the role of the aluminium species in the crystallization process.

2 Experimental

2.1 Sample preparation

The amorphous Al_2O_3–TiO_2–SiO_2 mixed oxides used as raw materials for the Al-TS-1 synthesis were prepared following a

two step sol–gel process described elsewere:[12–13] (1) acid-catalysed hydrolysis of the respective precursors, (2) basic condensation with TPAOH. The resulting solid was wetness-impregnated with aqueous 20 wt.% TPAOH solutions (1.6 g of TPAOH solution per 1 g of dried cogel). The crystallization of the incipient wet Al_2O_3–TiO_2–SiO_2 cogel was carried out in Teflon-lined autoclaves under autogenous pressure and static conditions at 170 °C for different times. After this treatment, the solid product was separated by centrifugation, washed several times with distilled water and dried overnight at 110 °C. The calcination of the samples was carried out in air at 550 °C for 7 hours. The synthesis yield (Y_s) was calculated as the weight of calcined solid relative to the weight of SiO_2 in the initial xerogel.

2.2 Characterisation

Chemical analyses were performed by X-ray fluorescence (XRF) with a PHILIPS PW 1480 spectrometer. X-Ray diffraction (XRD) patterns were collected with a PHILIPS X'PERT diffractometer with CuKα radiation. Fourier transform IR (FT-IR) spectra were recorded by means of a Nicolet 510P spectrophotometer using the KBr wafer technique. The crystallinity of the samples (X_c) was determined from both the XRD peak areas between $2\theta = 22$–25° and the ratio between the intensities (in absorbance units) of the 550 and 800 cm^{-1} IR bands, using a highly crystalline Al-TS-1 sample as reference.

Diffuse reflectance UV-VIS spectra (DR UV-VIS) were obtained under ambient conditions on a CARY-1 spectrophotometer equipped with a diffuse reflectance accessory. ^{29}Si and ^{27}Al magic angle spinning nuclear magnetic resonance (MAS-NMR) spectra of powdered samples were recorded at 59.57 and 78.14 MHz, respectively in a VARIAN spectrometer Model VXR-300. The spinning frequency was 4 kHz and intervals ranging from 5 to 30 s between successive accumulations were selected according to the crystallinity of the samples. Measurements were carried out at room temperature with tetramethylsilane (TMS) and $[Al(H_2O)_6^{3+}]$ as external standard references, with accumulations amounting to 2000 and 400 FIDs, respectively.

Nitrogen and argon isotherms at 77 K and 77.5 K, respectively, were determined using a volumetric adsorption apparatus equipped with a vacuum turbo-molecular pump for the determination of the pore size distribution in the microporous range (Micromeritics, ASAP 2010). The surface area was estimated according to the BET method. The pore size distribution in the mesopororous range was obtained by applying the BJH model with cylindrical pore geometry and using the Harkins and Jura equation for determining the adsorbed layer thickness. The pore size distribution in the microporous range was calculated using the Horvath–Kawazoe model for cylinder geometry (Saito/Foley). The morphology and size of the crystallites were determined by scanning electronic microscopy (SEM) with a JEOL JSM-6400 microscope.

The catalytic tests of n-hexane oxyfunctionalization were carried out in a magnetically stirred batch reactor equipped with a temperature controller and pressure gauge at 100 °C for 1 hour. All the reactants and the catalyst were charged into the Teflon-lined reactor and the system was heated to 100 °C. Aqueous H_2O_2 (30 wt% Panreac) was used as oxidant and methanol as solvent (H_2O_2/n-hexane molar ratio = 1.176, n-hexane/methanol mass ratio = 0.276, n-hexane/catalyst mass ratio = 12 and mass catalyst = 0.2 g). The H_2O_2 concentration after reaction was evaluated by iodometric titration. The catalytic test for acid-catalysed reactions (*tert*-butyl alcohol and methanol etherification) were carried out in analogous stirred autoclaves at 100 °C for 4 hours. Both alcohols and the catalyst were charged into the Teflon-lined autoclave (*tert*-butyl alcohol/methanol mass ratio = 1, *tert*-butyl alcohol/catalyst mass ratio = 7.5 and catalyst mass = 0.2 g) and then the system was heated to 100 °C. All the reaction products were analysed by gas chromatography (VARIAN 3380) on a capillary column HP-FFAP 60 m × 0.32 mm.

3 Results and discussion

In order to study the mechanism of Al-TS-1 crystallization under wetness-impregnation conditions, a kinetic run was carried out varying the synthesis time at 170 °C. The initial amorphous xerogel was a SiO_2–TiO_2–Al_2O_3 mixed solid with Si/Ti and Si/Al molar ratios of 60 and 120, respectively. This solid was impregnated with an aqueous solution of TPAOH (20 wt.%) until the incipient wetness point was reached.

Fig. 1(a) shows the crystallization kinetics corresponding to this experiment. An induction time of 2 hours can be clearly observed without any evidence of crystalline material detected by XRD (Fig. 1(b)); also confirmed by the absence of a band at 550 cm^{-1} in the IR spectra, typical of pentasil zeolites (Fig. 1(c)). This is followed for a second step with a high crystallization rate where the crystallinity changes from 0% to 100% in just 1 hour.

Fig. 2(a) shows the evolution of the solid yield along the progress of the crystallization. From these results, it is observed that the crystallization proceeds clearly through three different steps. The first one involves the partial dissolution of the initial xerogel leading to a decrease of synthesis yield from 100 to *ca.* 70% without any evidence of crystalline material. In the second step, the crystallinity changes from 0% to 90% whereas the solid yield remains constant. Finally, an increase in the yield up to *ca.* 85% is observed whereas the crystallinity changes from 90 to 100%.

The incorporation degree of the Ti and Al species into the solid phase along the synthesis is depicted in Fig. 2(b). The results indicate that the percentages of both elements in the solid decrease during the earlier stages of the process prior to the formation of the first crystalline products. However, it must be noticed that the decrease of the Al species is much less pronounced than that found for Ti species and the crystallization occurs with almost 100% of Al atoms initially incorporated into the raw SiO_2–TiO_2–Al_2O_3. However, after 2 hours of treatment at 170 °C, just 40% of the Ti atoms initially incorporated into the raw material are present in the amorphous solid (see Fig. 1(a) and 2(b)). This trend observed for Ti atoms is in fairly good agreement with the results reported by Serrano *et al.*[20] for TS-1 crystallization from wetness impregnated SiO_2–TiO_2 xerogels, where just 60% of the initial Ti atoms present in the initial xerogel were found in the solid prior to crystallization. It has been reported that there is a limit to the proportion of Ti and Al atoms that can be effectively incorporated into tetrahedral positions of the MFI structure corresponding to a Si/Ti molar ratio of 39 for pure TS-1[23] and a Si/Al molar ratio around 15 for ZSM-5. Owing to the difference in the affinity towards isomorphous substitution between Al and Ti atoms, almost all the aluminium present in the starting xerogel remains in the solid during the synthesis and it is completely incorporated into the final crystalline material. Additionally, this high Al incorporation limits the Ti content in the amorphous solid prior to crystallization and hence a higher dissolution of Ti species in comparison to that found for the TS-1 crystallization is evidenced.[20]

Once adequate amounts of Ti and Al species have been expelled from the solid during the first 2 hours of reaction, the Ti and Al contents remain almost constant in spite of the variation of the crystallinity from 0 to 90%. These results are the first evidence suggesting that most of the zeolite crystallization is not mediated by the solution phase. Only the last stage of the crystallization to reach 100% of crystallinity proceeds by incorporation of soluble species from the solution

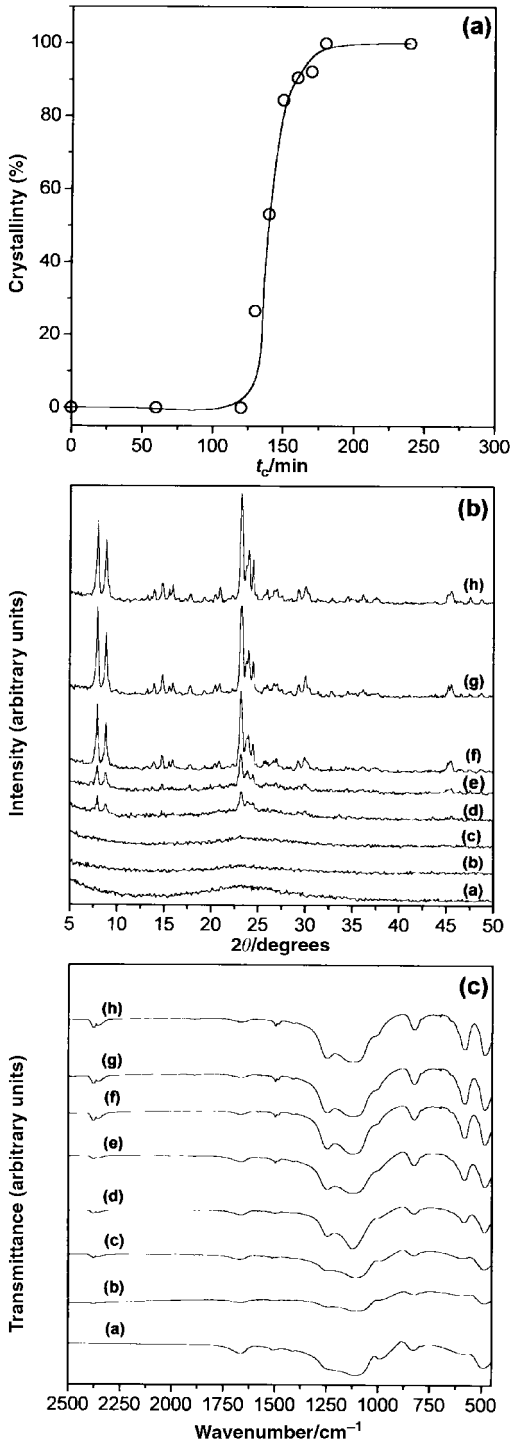

Fig. 1 (a) Crystallization kinetics of Al-TS-1. (b) XRD spectra and (c) FT-IR spectra of samples obtained at different reaction times: (a) 0 min, (b) 60 min, (c) 120 min, (d) 130 min, (e) 140 min, (f) 150 min, (g) 160 min, (h) 180 min.

with a complete incorporation of aluminium species and a significant enhancement in the percentage of Ti present in the solid phase.

^{29}Si MAS-NMR spectra of calcined samples at different degrees of crystallinity are depicted in Fig. 3. Having in mind the amorphous nature of the initial samples (synthesis times lower than 120 minutes), the ^{29}Si spectrum for the sample obtained at 60 min of synthesis is dominated by broad signals, which are gradually narrowing as the crystallization proceeds. The spectra exhibit clearly two broad features associated with Q^3 (−95.0 to –104.0 ppm) and Q^4 (−104.0 to *ca.* –115.0 ppm)

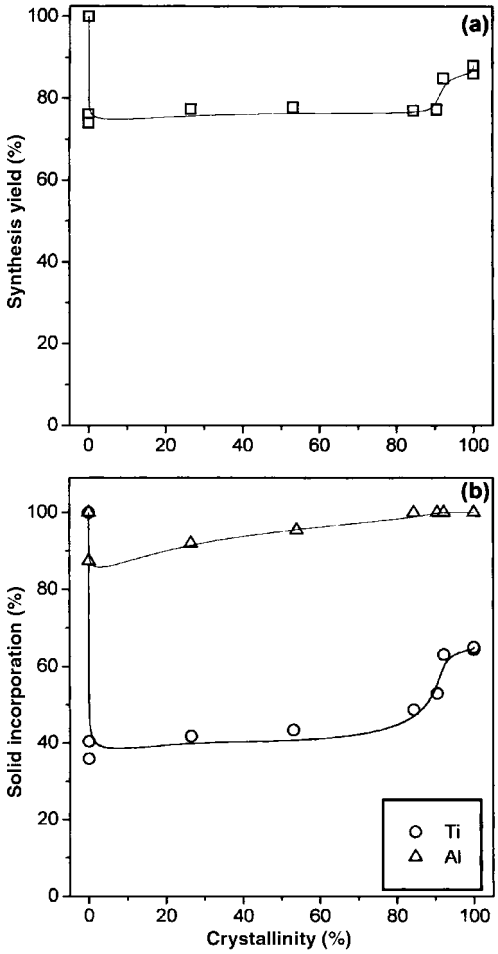

Fig. 2 (a) Synthesis yields along the crystallization. (b) Evolution of Ti and Al species in the solid phase during the synthesis.

Si connectivities.[24] Peaks in the Q^3 region are due to silanol groups, while those in Q^4 are attributed to Si connected to 4 T-atoms through O-atoms. Therefore, the decrease of the Q^3/Q^4 ratio obtained by deconvolution of the global signal and depicted in Fig. 3 *versus* the crystallinity (top left) reveals an

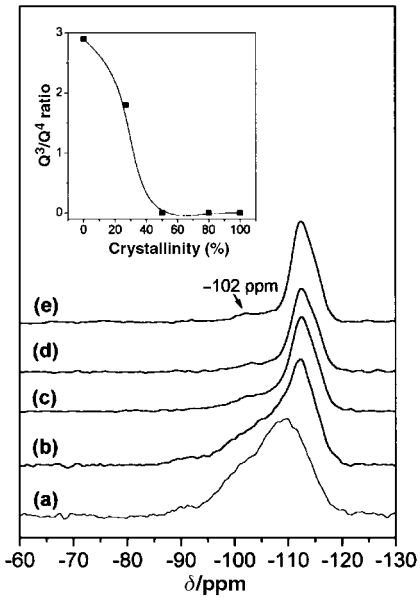

Fig. 3 ^{29}Si MAS-NMR spectra at different synthesis times and (inset) variation of Q^3/Q^4 ratio with the crystallinity for calcined samples: (a) 60 min, X_c=0%, (b) 130 min, X_c=27%, (c) 140 min, X_c=50%, (d) 150 min, X_c=84%, (e) 180 min, X_c=100%.

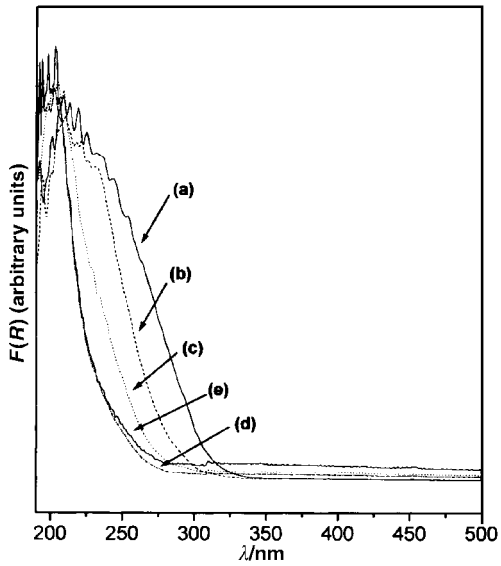

Fig. 4 DR UV-Vis spectra of calcined samples obtained at different synthesis times: (a) 0 min, $X_c = 0\%$, (b) 120 min, $X_c = 0\%$, (c) 130 min, $X_c = 27\%$, (d) 150 min, $X_c = 84\%$, (e) 180 min, $X_c = 100\%$.

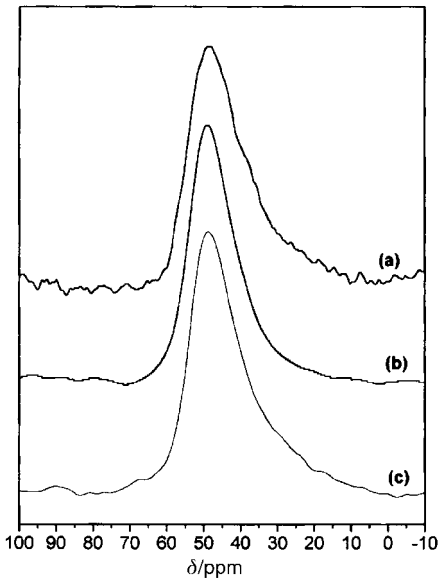

Fig. 5 ^{27}Al MAS-NMR spectra of calcined samples obtained at different synthesis times: (a) 0 min, $X_c = 0\%$, (b) 140 min, $X_c = 50\%$, (c) 180 min, $X_c = 100\%$.

increase of the condensation degree of silicon species with the progress of the crystallization.[24] The Q^3/Q^4 ratio decreases rapidly, with sharp changes occurring at the early stages of the crystallization ($X_c = 0$–50%). The complete condensation of silicon species for a crystallinity of 50% should be noted. Analogously, a significant change in the chemical shift of the centroid of the Q^4 feature from the amorphous material (-109.0 ppm) to the pseudo-crystalline and crystalline samples (-112.6 ppm) can be observed. This upfield shift reflects a decrease in Si–O bond lengths and increase in Si–O–Si bond angles during the transformation of the amorphous solid, which are consistent with the increasing of crystallinity.[24] Additionally, a signal centred at -102.0 ppm can be observed for the high crystalline materials, which is attributed to the Si–O–Al bond.[24]

Fig. 4 shows the DR UV-Vis spectra of the calcined samples obtained at different synthesis times, compared with that of the starting xerogel. In all cases, the absorption at 330 nm attributed to extraframework TiO_2[25] is negligible and a band centred at 220 nm is observed for all the samples showing that the Ti atoms are occupying tetrahedral positions.[25] In contrast with highly crystalline Al-TS-1, the initial xerogel presents a wide band ranging from 200 to 300 nm, showing that different Ti environments besides tetrahedral species coexist in this material with a lower degree of connectivity to the silica network. Therefore, as the Ti connectivity to the polymeric silica network increases, the corresponding DR UV-Vis absorption band must gradually shift towards lower wavelengths due to the presence of more homogeneous Ti environments. The amorphous material obtained after 120 minutes resulting from the partial dissolution of the initial xerogel presents a DR UV-Vis spectrum displaced towards lower wavelengths (Fig. 4b). This result suggests that the dissolution of Ti species during the induction time affects preferentially those with lower connectivity degrees to the silica network (wavelengths around *ca.* 275 nm). Beyond 120 minutes of synthesis, as the crystallization progresses, the spectra become narrower in spite of the fact that the amount of Ti present in the solid remains constant. Moreover, it is remarkable that the more significant changes in the spectra take place in the initial stages of the crystallization ($X_c = 0$–27), while the sample obtained at 130 min with low crystallinity ($X_c = 27\%$) exhibits a spectrum similar to that of the final crystalline Al-TS-1 (Fig. 4e).

Fig. 5 shows the ^{27}Al MAS-NMR spectra of three samples with different degrees of crystallinity. The spectra of the samples show only a signal centred at *ca.* 50.0 ppm associated with Al atoms in tetrahedral environments in the framework[26] with the complete absence of a peak at 0 ppm, which denotes that the samples are free of extraframework Al. Note the presence of Si–O–Al bonds in the starting amorphous material as well as Si–O–Ti bonds. The linewidth of the ^{27}Al MAS-NMR signals decreases along the crystallization with the most significant changes occurring in the early stages of the crystallization. The narrowing of the signal reflects the presence of more homogeneous Al environments consistent with the increase of the crystallinity.

The samples prepared at different synthesis times have been checked as bifunctional catalysts in the n-hexane oxyfunctionalization with H_2O_2 and methanol as solvent, as well as in the etherification of *tert*-butanol and methanol. The results obtained are summarised in Tables 1 and 2 respectively. The

Table 1 Oxidation of n-hexane with H_2O_2 using methanol as solvent

					Molar product distribution			
Time/min	X_c (%)	$X_{\text{n-hexane}}{}^a$	$X_{\text{oxidant}}{}^b$	$S_{\text{oxidant}}{}^c$	3-Hexanone	2-Hexanone	3-Hexanol	2-Hexanol
120	0	0	14.7	0	0.0	0.0	0.0	0.0
130	27	9.7	45.0	23.1	0.0	33.6	24.4	42.0
140	53	23.3	52.3	54.0	5.7	45.9	20.1	28.2
150	84	30.1	67.1	56.3	6.2	50.7	20.4	22.7
180	100	41.2	71.8	75.7	23.1	41.9	17.9	17.2

[a]n-Hexane conversion defined as: reacted n-hexane/fed n-hexane × 100. [b]Oxidant conversion defined as: reacted H_2O_2/fed H_2O_2 × 100. [c]Oxidant selectivity defined as: (2 × mol hexanones + mol hexanols)/reacted H_2O_2 × 100.

Table 2 Etherification of *tert*-butanol and methanol

			Molar products distribution	
Time/min	X_c (%)	$X_{tert\text{-butanol}}$[a]	MTBE	Isobutene
120	0	5.6	0.0	100
130	27	23.3	1.6	98.4
140	53	39.4	28.9	71.1
180	100	58.1	36.2	63.8

[a]*tert*-Butanol conversion defined as: reacted *tert*-butanol/fed *tert*-butanol × 100.

oxidation catalytic tests show that the amorphous material obtained after 120 minutes of synthesis does not exhibit any activity for n-hexane oxidation and only promotes the oxidant decomposition into water and oxygen. The n-hexane oxidation occurs for samples having a certain macroscopic crystallinity, the substrate conversion and the oxidant selectivity being well correlated with the proportion of crystalline material present in each sample. Likewise, the Ti environment influences not only the activity but also the molar distribution of products, a higher amount of hexanones being obtained as the sample crystallinity increases. These results suggest that the activity of the Ti centres is directly related to their incorporation in tetrahedral positions in the crystalline framework, since the Ti centres located in amorphous structures are not active, even when located in tetrahedral environments. Similar behaviour is found for the acid centres in the acid-catalysed reaction shown in Table 2; the amorphous material presents a low activity, which is clearly enhanced as the crystallinity of the samples increases. Moreover, the evolution of the product distribution clearly indicates that the strength of the acid centres is tuned as the Al environments are modified along the crystallization. Although DR UV-Vis, ^{29}Si and ^{27}Al NMR characterisation results show that the Ti and Al coordination as well as the condensation degree of silicon species for the sample with a crystallinity of 50% are similar to those found for the highly crystalline material, their catalytic activity is significantly different. The catalytic results show that the activity of Al and Ti centres is clearly related to the progress of the crystallization, since the crystalline environment seems to be essential for the catalytic activity.

In order to follow the changes undergone by the solid through the variation of its textural properties, N_2 adsorption/desorption isotherms were measured at 77 K for calcined samples prepared for different synthesis times. Fig. 6(a) shows the corresponding isotherms and Table 3 presents the BET surface areas, micropore surfaces and micropore volumes of the samples. The isotherm and textural properties corresponding to the raw xerogel indicate that this material is mesoporous, most of the N_2 adsorption being observed at high P/P_o. In contrast, the isotherm corresponding to the amorphous material obtained at 120 minutes, although with an important mesoporosity presents a significant amount of micropores as concluded from the presence of a micropore volume of 0.11 $cm^3\ g^{-1}$ as estimated by the *t*-plot method. As the crystallization progresses, increasing microporosity is observed until a micropore volume around 0.19 $cm^3\ g^{-1}$ is reached for the highly crystalline materials in close agreement to that corresponding to a pure MFI structure. Note that these changes in the micropore volume are more significant after *ca.* 50% crystallinity was reached. Fig. 6(b) shows the pore size distribution in the mesopore range of the different samples calculated using the BJH model. The amorphous materials show a maximum centred on a pore diameter around 110 Å corresponding to the presence of mesopores, which disappears completely along the crystallization. A more in-depth study of the sample microporosities was carried out by means of Ar adsorption isotherms at 77.5 K over calcined samples with 0% (120 min), 50% (140 min) and 100% (180 min) crystallinity (Fig. 6(c)). These measurements confirm the results obtained with the nitrogen adsorption/desorption measurements showing an increase of microporosity with the crystallization

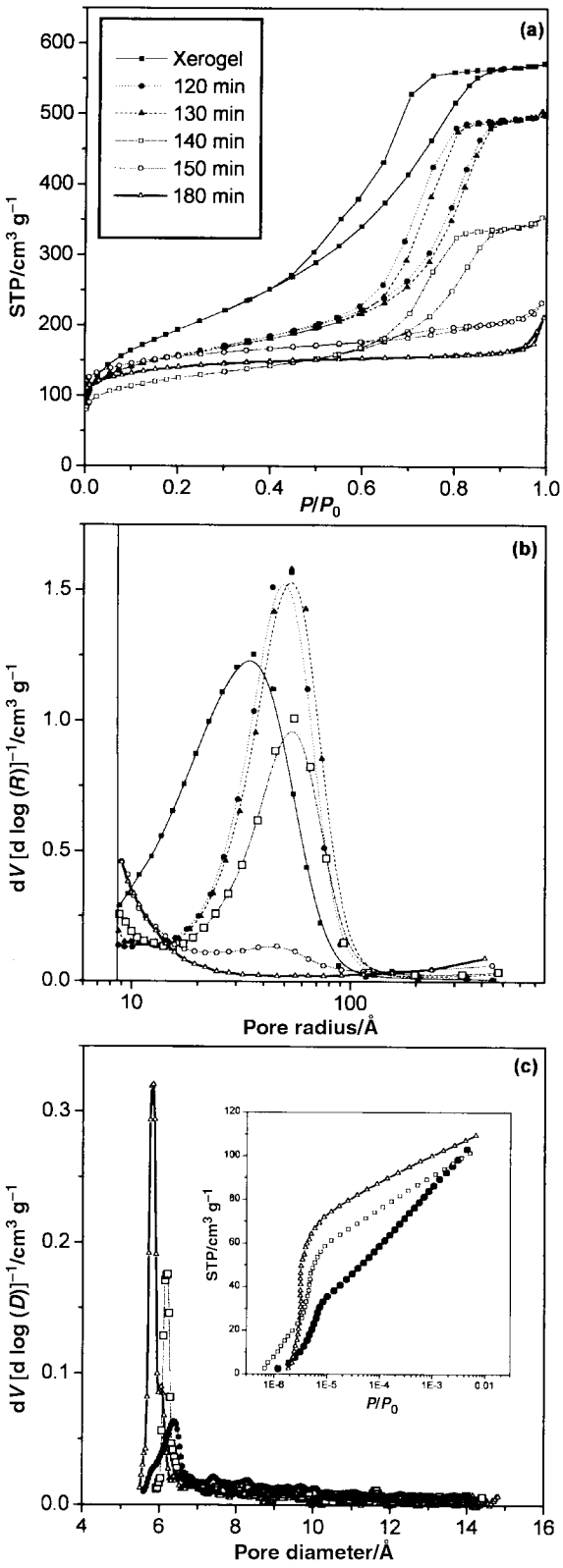

Fig. 6 (a) Nitrogen adsorption/desorption isotherms at 77 K of samples obtained at different synthesis times, and (b) their corresponding mesopore size distributions. (c) Argon adsorption isotherms at 77.5 K of samples synthesised at different crystallization times (inset) and their corresponding micropore size distributions.

Table 3 Textural properties of samples at different synthesis times

Time/ min	X_c (%)	BET surface/ $m^2\ g^{-1}$	Micropore surface/$m^2\ g^{-1}$	Micropore volume/$cm^3\ g^{-1}$
Xerogel	0	689.0	26.0	0.01
120	0	540.5	224.2	0.11
130	27	534.3	239.4	0.12
140	53	524.1	320.8	0.15
150	84	535.0	436.3	0.19
180	100	490.0	427.1	0.19

process. Furthermore, this increase of microporosity is accompanied by a narrow pore size distribution and a shifting of the average pore diameter to lower values. The sample with 100% crystallinity shows an average pore diameter of *ca.* 5.8 Å in fairly good agreement with that reported for a pure MFI structure of 5.5 Å.

Fig. 7 shows SEM micrographs recorded on samples with different crystallinity degrees. Fig. 7(a) shows the amorphous material obtained from partial dissolution of the initial xerogel constituted of very small primary particles with sizes around 0.1 μm. As the crystallization progresses (Fig. 7, (b) and (c)), new larger particles (secondary units) formed by aggregation of the primary ones appear, being in contact with the cogel surface. The appearance of these secondary units is directly linked to the observance of macroscopic crystallinity. These secondary particles grow and become independent when reaching a critical diameter of *ca.* 0.5 μm. During this stage of the crystallization it must be noticed that the solid yield and Ti and Al contents in the solid remain constant until reaching a crystallinity of *ca.* 90%. The SEM images confirm the earlier conclusions, the zeolitization of the secondary particles takes place mainly through solid–solid transformations which allow the amorphous network to be reordered into the zeolite framework. The classical step of crystal growth around the previously formed nuclei by incorporation of soluble species is not valid to describe this system. In the last stage of the crystallization to reach 100% crystallinity, these particles are transformed into crystals of the same size through a process mediated by the incorporation of soluble species of Ti, Si and Al from the solution. In this last stage, the increase of the yield is balanced by the packing of the particles and hence there is no evidence of a significant increase in the final crystal size (Fig. 7(e)). This crystallization mechanism resembles that found for the TS-1 zeolite starting from SiO_2–TiO_2 wetness-impregnated xerogels,[20] although greater participation of the solution-mediated process is evidenced in the last stage of the crystallization.

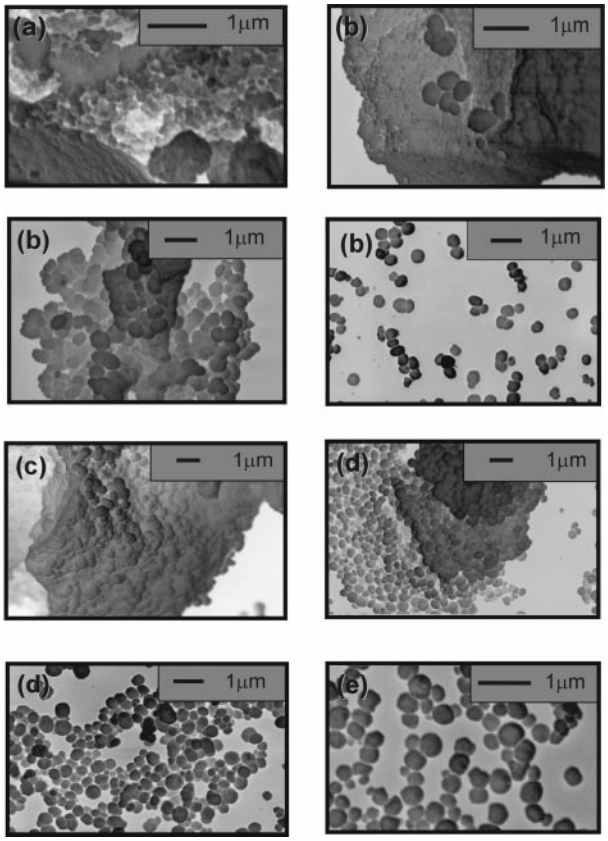

Fig. 7 SEM images of samples with different crystallinities: (a) 120 min, $X_c = 0\%$, (b) 130 min, $X_c = 27\%$, (c) 140 min, $X_c = 50\%$, (d) 150 min, $X_c = 84\%$, (e) 180 min, $X_c = 100\%$.

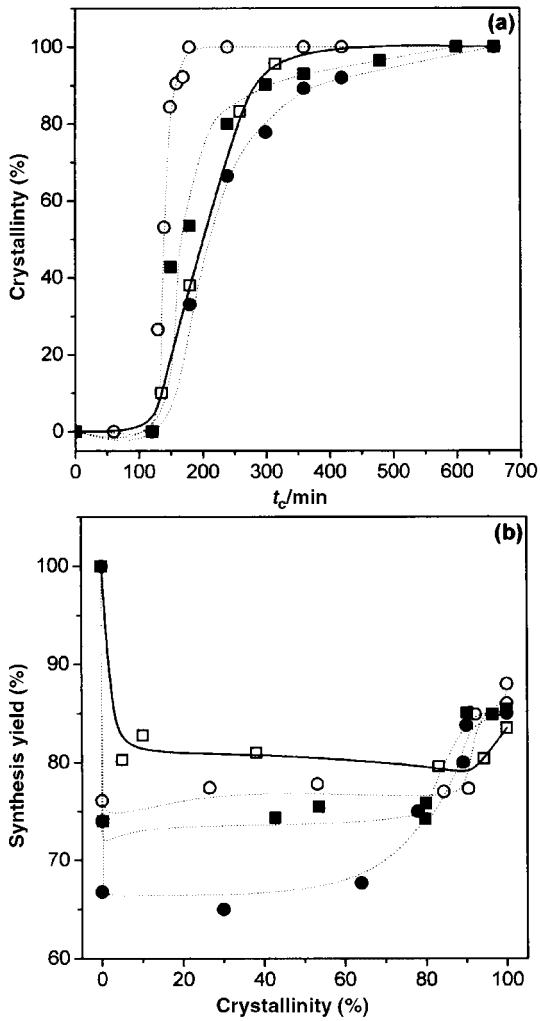

Fig. 8 Crystallization of Al-TS-1 samples with different Al content in the initial xerogel: (○) Si/Ti = 60 and Si/Al = 120, (□) Si/Ti = 60, (■) Si/Ti = 60 and Si/Al = 80, (●) Si/Ti = 60 and Si/Al = 60. (a) Kinetic curves, (b) synthesis yields.

Finally, we have increased the amount of aluminium in the initial xerogel in order to elucidate its role in this non-conventional crystallization mechanism. In this way, two additional kinetic runs were carried out starting from Al_2O_3–SiO_2–TiO_2 wetness-impregnated xerogels with an Si/Ti molar ratio of 60 and Si/Al molar ratios of 80 and 60, respectively. A kinetic run starting from SiO_2–TiO_2 wetness-impregnated xerogels with an Si/Ti molar ratio of 60 was also carried out. Fig. 8(a) shows the crystallization kinetics corresponding to these experiments, including that shown in Fig. 1 starting from an Al_2O_3–SiO_2–TiO_2 wetness-impregnated xerogel with Si/Ti and Si/Al molar ratios of 60 and 120, respectively.

The three kinetic runs show an induction time of 2 hours followed by a second step where the crystallization rate seems

to be influenced by the Al content in the initial xerogel. A remarkable fact is that the crystallization rate for the sample starting from impregnated xerogels with the lowest Al content (Si/Al molar ratio of 120) is faster than that found for the TS-1 crystallization starting from xerogels with similar Ti content and no Al species. As was mentioned before, for this sample 100% crystalline materials are obtained in just 3 hours whereas this process may be extended to 6 hours for the synthesis of TS-1.[20] However, when the aluminium content is increased in the initial xerogel (Si/Al molar ratios of 80 and 60, respectively) a delay in the last stage of the crystallization is readily evidenced.

Fig. 8(b) compares the synthesis yields for the different kinetic runs *versus* the crystallinity. For the three kinetic runs a similar trend to that reported for the sample starting from amorphous xerogels with a Si/Al molar ratio of 120 is observed. An initial xerogel dissolution step is found, which is enhanced as the Al content increases in the initial xerogel. These data seem to indicate that high Al contents lead to more reactive starting amorphous xerogels. This initial step is followed by a second one where the yield remains constant along the crystallization up to values set by the Al content in the initial xerogel. In this way, for the TS-1 sample the yield remains almost constant until crystallinity values of 95% are reached. However, this final point is gradually shifted to lower values as the Al content increases in the starting wetness-impregnated xerogel. The third step involves the yield increase by incorporation of soluble species from the solution, reaching similar values in all cases independent of the Al content in the initial xerogel. From the data depicted in Fig. 8, the significant influence of the aluminium content in the initial xerogel on the progress of the zeolite crystallization can be clearly seen. An increase of the Al content enhances the reactivity of the solid towards dissolution, providing more soluble species and making more relevant the participation of the solid-mediated processes in the Al-TS-1 crystallization.

The evolution of Al and Ti incorporation into the solid along the crystallization for the different samples show that almost all the initial Al content remains in the solid after the partial xerogel dissolution. However, the dissolution of Ti species is dramatically enhanced with the increase of the Al incorporation in the starting material. This difference of solubility of the Ti and Al species could be related to their distinct affinity towards the isomorphous substitution previously discussed.[14]

XPS measurements performed on different crystalline Al-TS-1 samples synthesised from xerogels with varying Al content and constant Ti, described in a previous work,[14] showed significant Ti composition gradients into the zeolite when Al is present, this fact being more pronounced at higher Al content in the initial xerogel. These composition profiles can be easily explained according to the crystallization mechanism described in this work, where an important incorporation, mainly of the Si and Ti species from the solution, is evidenced in the last stage of the crystallization as the Al content increases in the initial xerogel.

4 Conclusions

According to the results obtained, the Al-TS-1 crystallization mechanism from amorphous wetness-impregnated Al_2O_3–TiO_2–SiO_2 xerogels can be described as follows. The starting polymeric xerogel is partially dissolved during the first hours of synthesis to yield a particulate material formed by amorphous primary particles with sizes around 0.1 μm. This dissolution affects mainly the Ti and Si species. Thereafter, the primary particles undergo an aggregation process on the amorphous cogel particles leading to the formation of larger units (secondary particles). The latter are separated from the cogel as they reach a critical diameter of *ca.* 0.5 μm. At this point, the first signs of long-range crystallinity are detected. This solid phase is rich in aluminium species, which limits the presence of Ti in the solid. This stage proceeds mainly through solid–solid transformations with deep changes occurring in the Al, Ti and Si environments. At the end of this step, the conversion of the cogel into secondary particles is completed. Finally, the secondary particles are gradually transformed into Al-TS-1 crystals through incorporation of soluble species from the solution. This step is the slowest one in the overall process, mainly governed by liquid phase transport.

In agreement with this scheme, Al-TS-1 crystallization from amorphous Al_2O_3–TiO_2–SiO_2 xerogels proceeds by a non-conventional mechanism. In the system here studied, solid–solid transformations of the amorphous network have an important relevance in the formation of the Al-TS-1 crystals. The increase of the Al content in the initial xerogel has a dramatic influence on the different steps of the overall process: enhancement of the Si and Ti species dissolution during the first step; limitation of the presence of Ti incorporated into the solid; enhancement of the participation of solution-mediated processes in the overall crystallization, which leads to slower kinetics and significant composition gradients within the crystals.

References

1 M. Taramasso, G. Perego and B. Notari, *US Pat.*, 4410501, 1983.
2 P. Roffia, M. Padovan, E. Moretti and G. D. Alberti, *Eur. Pat. Appl.*, 208311, 1987.
3 D. R. C. Huybrechts, L. D. Bruycker and P. A. Jacobs, *Nature*, 1990, **345**, 240.
4 A. Tuel, S. Moussa-Khouzami, Y. Ben Taârit and C. Naccache, *J. Mol. Catal.*, 1991, **68**, 45.
5 M. G. Clerici, G. Bellusi and U. Romano, *J. Catal.*, 1991, **129**, 159.
6 A. Thangaraj, R. Kumar and P. Ratnasamy, *J. Catal.*, 1991, **131**, 394.
7 B. Notari, *Catal. Today*, 1993, **18**, 163.
8 G. Bellusi, A. Carati, M. G. Clerici and A. Esposito, *Stud. Surf. Sci. Catal.*, 1991, **63**, 241.
9 L. Forni, M. Pellozi, A. Giusti, G. Fornasari and R. Millini, *J. Catal.*, 1990, **122**, 44.
10 A. Thangaraj, R. Kumar and S. Sivasanker, *Zeolites*, 1992, **12**, 135.
11 D. Trong On, S. Kaliaguine and L. Bonneviot, *J. Catal.*, 1995, **157**, 235.
12 G. Ovejero, R. Van Grieken, M. A. Uguina, D. P. Serrano and J. A. Melero, *Catal. Lett.*, 1996, **41**, 69.
13 G. Ovejero, R. Van Grieken and J. A. Melero, *Microporous Mesoporous Mater.*, 1998, **22**, 638.
14 G. Ovejero, R. van Grieken, M. A. Uguina, D. P. Serrano and J. A. Melero, *J. Mater. Chem.*, 1998, **8**, 2269.
15 M. A. Uguina, G. Ovejero, R. van Grieken, D. P. Serrano and M. Camacho, *J. Chem. Soc., Chem. Commun.*, 1994, 27.
16 D. P. Serrano, M. A. Uguina, G. Ovejero, R. van Grieken and M. Camacho, *Microporous Mater.*, 1995, **4**, 273.
17 M. A. Uguina, D. P. Serrano, G. Ovejero, R. van Grieken and M. Camacho, *Appl. Catal. A*, 1995, **124**, 391.
18 R. van Grieken, G. Ovejero, D. P. Serrano, M. A. Uguina and J. A. Melero, *Chem. Commun.*, 1996, 1145.
19 R. van Grieken, G. Ovejero, D. P. Serrano, M. A. Uguina and J. A. Melero, *Ind. Eng. Chem. Res.*, 1998, **37**, 4215.
20 D. P. Serrano, M. A. Uguina, G. Ovejero, R. van Grieken and M. Camacho, *Microporous Mater.*, 1996, **7**, 309.
21 D. P. Serrano, M. A. Uguina, G. Ovejero, R. van Grieken and M. Camacho, *Chem. Commun.*, 1996, 1907.
22 D. P. Serrano, M. A. Uguina, G. Ovejero, R. van Grieken, M. Camacho and J. A. Melero, *J. Mater. Chem.*, 1999, **9**, 2899.
23 R. Millini, E. P. Massara, G. Perego and G. Bellussi, *J. Catal.*, 1992, **137**, 497.
24 G. Engelhardt and D. Michel, *High Resolution Solid-State NMR of Silicates and Zeolites*, Wiley, Chichester, 1987.
25 F. Geobaldo, S. Bordiga, A. Zecchina, E. Gianello, G. Leofanti and G. Petrini, *Catal. Lett.*, 1992, **16**, 109.
26 A. D. Irwin, J. S. Holmgren and J. Jonas, *J. Mater. Sci.*, 1998, **23**, 2098.